The impact of photocatalytic paint porosity on indoor NOx and HONO levels

Adrien Gandolfo, Vincent Bartolomei, Delphine Truffier-Boutry, Brice Temime-Roussel, Gregory Brochard, Virginie Bergé, Henri Wortham, Sasho Gligorovski

The impact of photocatalytic paint's porosity on indoor NOx and HONO levels

Adrien Gandolfo[a,*], Vincent Bartolomei[b,1], Delphine Truffier-Boutry[b,2], Brice Temime-Roussel[a], Gregory Brochard[c], Virginie Bergé[c], Henri Wortham[a], Sasho Gligorovski[d,*]

[a]Aix Marseille Univ, CNRS, LCE, UMR 7376, 13331 Marseille, France

[b]Université Grenoble Alpes, CEA, Laboratoire en Nanosécurité et Nanocaractérisation, Grenoble, France.

[c]ALLIOS, Les Docks Mogador, 105 chemin de St Menet aux Accates, 13011 Marseille, France

[d]State Key Laboratory of Organic Geochemistry, Guangzhou Institute of Geochemistry, Chinese Academy of Sciences, Guangzhou 510 640, China

[1]Now at …

[2]Now at…

Abstract

1. Introduction

Indoor pollutant concentrations are considered to be one order of magnitude higher than in the free troposphere [1]. Among them, volatile organic compounds (VOCs) and nitrogen oxides (NOx) are dominant and may exert adverse health effects [2]. Thus, indoor environments are usually considered as potentially risky environments according to the environmental protection agencies [3,4]. The second major concern of indoor environments is energy consumption. New directives set objectives with the aim of reducing energy consumption resulting in the construction of high-efficiency low-energy buildings in developed countries [5]. Such buildings are more air-tight, potentially leading to pollutant accumulation and thus increase health risks for the inhabitants [6]. Among technologies which have been developed to clean the indoor pollutants, TiO_2 based photocatalytic remediation process received large attention [7–13] due to its reasonable cost, high stability, good efficiency, and chemical and biological inertia [10]. Under sufficient energy radiation (< 387 nm, i.e. > 3.2 eV), TiO_2 semiconductor activation occurs producing an electron-hole (e^-/h^+) pair on the photocatalyst surface which will further participate in redox surface reactions of adsorbed compounds [14].

In the last two decades, photocatalytic paints with embedded TiO_2 nanoparticles were available on the market. However, investigations of their efficiencies toward VOCs and NOx pollution are scarce [15–24]. In our previous studies, we observed NO_2 abatement by indoor photocatalytic paints in good agreement with other studies [15,17–20]. The efficiency of photocatalytic paints towards indoor pollutants is dependent on numerous parameters including the quantity of nanoTiO_2 embedded in paints, light intensity, surface temperature, and relative humidity (RH). Although promising results have been obtained toward removal of pollutants, some shortcomings still remain, such as formation of nitrous acid (HONO) and production of toxic aldehydes during the light irradiation of the photocatalytic paints.

[15,18,25,26]. The later implies that photocatalytic paints based on TiO_2 as a photocatalyst still need serious optimization to ensure safe use prior to being launched on the market.

One of the limitations of TiO_2 based photocatalytic paints is their low adsorption capacities [27]. To counterbalance this drawback, intense efforts have been made to load TiO_2 on absorbent supporting medium e.g. graphene structure, activated carbon or zeolite to improve TiO_2 effectiveness [28–30]. Overall, the efficiency is increased by the modification of the photocatalyst supporting medium. It is attributed (1) to the rise of the reaction surface area of the photocatalytic material, (2) the availability of photocatalyst within the medium and (3) the increased contact time between the gas and the photocatalyst. In building materials, attempts have been made in changing surface morphology to obtain the desired performance of photocatalytic materials mentioned above. Giosuè et al (2017) improved standard paints remediation capacity through the management of adsorption properties by changing siliceous filler with ones having higher porosity and specific surface area [31]. Sugranez et al (2013) changed the component ratio and the protocol for preparing mortar cement. As a consequence microstructure properties of the resulting material provided higher porosity without impacting the mechanical performance and achieved improvement on nitric oxide (NO) remediation [32,33]. Then, the larger specific surface area of FN2 coating (Advanced Materials-JTJ which consist in 74 % of Aeroxide TiO_2 P25 and 26 % of mineral binder) than pure Aeroxide TiO_2 P25 (Evonik) is responsible for the "more open texture" observed on SEM images of both coatings [34]. This particular texture allows better photocatalytic degradation of NOx in ISO 22197-1 flow reactor [34]. As a consequence, it would be expected that an increase in porosity of building materials would improve the photocatalytic performance.

In this study, we evaluate the efficiency improvement of indoor photocatalytic paints by increasing the pigment volume concentration (PVC) of the paints with the objectives to create a more open texture and/or porous material. Then, we assess the removal efficiency of these

paints towards NO_2 by investigating the NO_2 heterogeneous reactivity in a well-established flow tube reactor on 1) a non-photocatalytic white paint, thereafter, called reference paint and 2) photocatalytic paint. We discuss the formation of reaction by-products NO and HONO which are observed during the NO_2 degradation by the photocatalytic paints considered in this study. We also present surface emission fluxes of formaldehyde and acetaldehyde from the photocatalytic degradation of the organic binder. Finally, based on the observed results we suggest a strategy to be adopted in order to further improve these photocatalytic paints towards NOx and VOCs removal in indoor environments.

2. Experimental

2.1. Flow tube photo-reactor

A horizontal flow tube photo-reactor was used to investigate the NO_2 heterogeneous reactivity on photocatalytic paints considered in this study. The method has been widely used in the past for determination of kinetic parameters for the reactions of gas phase oxidants and solid phase such as soot, organic matter, ice, mineral dust, paints [18,35–41]. The flow tube reactor used in this study has already been described in our previous study [18,42]. It consists of a double-wall cylindrical borosilicate glass tube connected to a thermostated bath. The flow tube is 34 cm long with an internal diameter of 2.25 cm in which the glass plate (29 × 1.9 cm) covered on one side with paint perfectly fits into the glass tube. Bath temperature and thus surface temperature of the glass plates was kept constant at 23°C for all experiments [43]. A movable injector is inserted inside the reactor to introduce gaseous NO_2. By varying the length of the exposed paint surface to NO_2 under constant flow, we can access to the determination of the pseudo-first order kinetics. Specific positions are marked on movable injector resulting in known surface paint exposition of P1: 7.4 cm^2, P2: 14.8 cm^2, P3: 29.6 cm^2 and P4: 44.4 cm^2. The reactor is placed in a stainless-steel box where UV Lamps (Philips TL-D 18 W, 340–400 nm, λmax = 368 nm, length = 60 cm) are mounted on the top of the box to simulate sunlight

irradiation in the UV-range of 340-400 nm. The spectral irradiance of the lamps has already been characterized in a previous study [40]. To simulate the sunlit place in an indoor environment, an integrated spectral irradiance between 340 and 400 nm of 8.8 W m^{-2} was chosen and kept constant in all experiments.

2.2. Materials

2.2.1. Preparation of the paint

Our industrial partner within the LABEX consortium [44], the ALLIOS Company, supplied the paints. The paint chemical composition, the photocatalyst used, and the application procedure are described previously in details [18,26,45]. Briefly, all the paints are mainly constituted of structural agents, i.e. calcium carbonate, white pigments, i.e. TiO_2 in micrometric size, and organic binder. In order to formulate photocatalytic paints, a mixture of grinded additives was prepared with active TiO_2 nanoparticles (TITANE P2 in anatase form containing approximatively 85% of TiO_2). The slurry is added with the other above-mentioned paint constituents to reach 7 % of photocatalytic active TiO_2 nanoparticles (w/w). The additive mixture is absent of the non-photocatalytic paint which was used as a reference paint in the study. The prepared paint is then applied on a glass plate and dried following a well-established procedure resulting in a uniform thickness film [18].

To investigate the impact of paint porosity on the photocatalytic activity, the paint chemical composition remained unchanged while component volumetric ratio varied. Thus, the porosity variation is achieved through the variation of the pigment volume concentration (PVC). According to the ISO 4618-1 (1998), PVC is defined as the ratio of charges and pigments sum to the charges, pigments, and binder sum, as follows: [46].

$$PVC(\%) = \frac{Volume_{charges+pigments}}{Volume_{charges+pigments+binder}} \qquad \text{(Eq-1)}$$

Three paints with 53 %, 72 % and 82 % of PVC have been studied. To assess the paint porosity, it is necessary to introduce a specific PVC value named critical pigment volume concentration (CPVC). CPVC is a specific PVC in which the voids between the solid particles (structural agents and pigments) are just filled with the binder. Paints having a PVC higher than the CPVC, exhibit non-occupied volume in the bulk and a porosity according to the following equation:

$$Porosity(\%) = 1 - (\frac{CPVC}{PVC}) \quad \text{(Eq-2)}$$

Although CPVC was not known for the considered photocatalytic paint according to the manufacturer, CPVC is ~ 50-60 % for standard flat white paint. Thus, without being able to clearly state the paint porosity, we can assume that paints with 72 % PVC has greater porosity than paints with 53 % and that paints with 80 % PVC has greater porosity than others. Therefore, PVC term is preferred instead of porosity and will be used hereafter.

2.2.2. Gas supply

A pressurized cylinder tank containing 100 ppm of certified NO_2 diluted in helium (Linde gas, France) was used to provide the desired NO_2 mixing ratio during all the experiments. Synthetic air (Linde gas 5.0, France) was used as a carrier gas in the flow tube reactor. In order to obtain representative indoor NO_2 mixing ratio, the certified NO_2 mixture in helium underwent a first dilution step in a mixing loop to achieve a mixing ratio of 2 parts per million (ppm). Then, 20 ml min^{-1} of this stream (flow controller, Brooks SLA, 0–20 ml/min) was introduced in the reactor through the injector where a second dilution step took place in the carrier flow (980 ml min^{-1} of synthetic air, flow controller Brooks SLA 0–1 l min^{-1}). The total flow of 1 l min^{-1} drifts in the reactor, allowing laminar flow conditions. Finally, an initial NO_2 mixing ratio of 40 parts per billion (ppb) was reached and was used for the whole set of experiments. Before entering the reactor, the carrier gas flow passed through a humidification system which allows the variation of the air relative humidity in a range between 0 to 80 %.

Downstream of the reactor, a hygrometer “Hygrolog NT2” (Rotronic) with a “HygroClip SC04” probe measured the resulting humidity on-line (± 1.5 % RH accuracy).

2.3. Instruments

The mixing ratios of NO_x (NO_2 + NO) was monitored online by a chemiluminescence instrument (Eco Physics, model CLD 88p) coupled to a NO_2 to NO photolytic converter (Eco Physics, model PLC 860). The instrument operated under a flow of 730 ml min^{-1} and had a detection limit of 300 ppt. Gaseous HONO was measured with a Long Path Absorption Photometer (LOPAP-03 QUMA) under an operation gas flow of 990 ml min^{-1} and a liquid pump circulation of 20 rounds per minutes. The detail instrument description and performances are available in reference papers on the instrument development [47–49]. In our operational conditions, the instrument had a detection limit of 3 to 5 ppt.

3. Results

3.1. Characterization of photocatalytic paints

Images of the paint samples were acquired with an ultrahigh resolution scanning electron microscopy (UHR-SEM) as described in Truffier et al (2017) [45]. Photocatalytic paints containing 7 % of nanoTiO_2 with three various PVCs, i.e. 53 %, 72 %, and 80 % were observed by UHR-SEM (Figure 1). As mentioned above (section 2.2.1.), the paint porosity increases as the PVC increase.

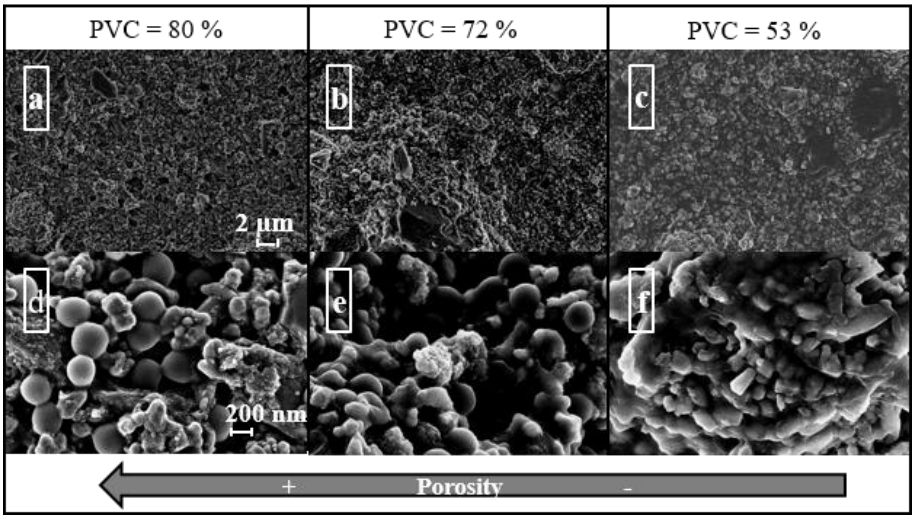

Figure 1: SEM observations of photocatalytic paint containing 7 % of nanoTiO_2. Applied magnifiers are 10^4 and 10^5 on the upper and lower panels respectively. Images (a) and (d), (b) and (e), and, (c) and (f) are paints with 80, 72 and 53 % PVC respectively.

Upper panel (a, b and c) show images magnified 10^4 times. Under this resolution, paint with 53 % PVC (c in Figure 1) has a higher opacity than paint with 72 and 80 % PVC (a and b in Figure 1). The optical phenomena are induced by the high proportion of binder in comparison to charges creating a masking effect on the paint surface. This observation is confirmed by picture f on the lower panel in Figure 1 (magnifier × 10^5). Clearly, $CaCO_3$ balls which are used as architectural structuring agent are embedded in the binder of paint with 53 % PVC. As the PVC increase, the binder is less present, and charges appear (e in Figure 1). This observation is accentuated for the paint with 80 % PVC where voids began to be seen. The structural changes induced by the increase of PVC and their effect on the NO_2 heterogeneous reactivity were assessed and are presented in the following sections.

3.2. Kinetic parameters

A typical NO_2 signal observed during the heterogeneous reactivity is presented in Figure 2 for the reference paint and paint containing 7 % of photocatalyst, both having a PVC of 80 %.

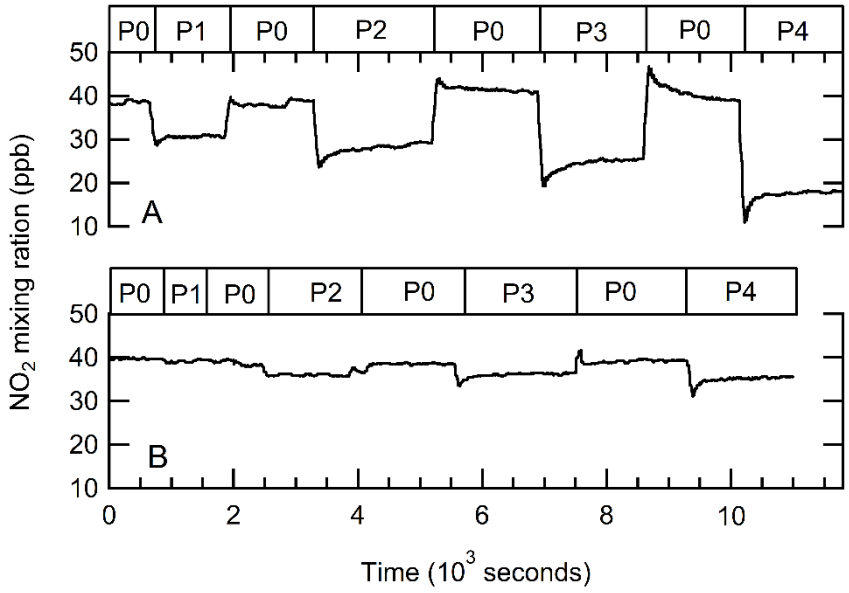

Figure 2: A typical signal of NO_2 during an experiment performed in the flow tube reactor, A) in presence of photocatalytic paint (7 %), , and B) on reference paint. Annotation P0, P1, P2, and P4 refer to movable injector position in the reactor. Experimental conditions were set to initial NO_2 mixing ratio of 40 ppb, RH 40 %, irradiation of 8.8 W m^{-2} (integrated between 340 and 400 nm), and surface temperature of 23 °C.

The position P0 in Figure 2 indicates a stable NO_2 mixing ratio of 40 ppb (C_0) reached after several hours of stabilization. Once the signal is stabilized, the injector is pulled to a known position e.g. P1 and kept in this position for several minutes (typically 30 minutes). At this moment, a quick drop can be observed in the NO_2 mixing ratio corresponding to the first contact between the paint surface and NO_2. Then, slowly, the signal slightly increased and reached a plateau at a mixing ratio lower than C_0. Once the signal is stabilized in this position, the injector is pushed back to the initial position P0 and NO_2 mixing ratio decreases to C_0. This action is repeated four times by varying the movable injection position in the reactor (i.e. P1, P2, P3, and P4). The comparison between Figure 2A and 2B shows that the NO_2 consumption is much higher on the photocatalytic paint due to the embedded TiO_2 nanoparticles [18]. The NO_2 consumption follows a pseudo-first order kinetics. The measured first-order rate constant can be used to estimate the uptake coefficients of NO_2 as follows [18]:

$$\gamma = \frac{4k_{obs}}{\bar{v}S/V} \quad (3)$$

Where k_{obs} (s^{-1}) is the first-order rate constant of the reaction. S and V are the surface (cm^2) and volume (cm^3) of the reactor, respectively, and $\bar{\upsilon}$, the mean NO_2 velocity (cm s^{-1}). Uptake coefficient measurements might be limited by the gas-phase diffusion processes in flow tube reactors under laminar flow conditions [50,51]. This limitation leads to an underestimation of the uptake coefficient for too high reactivity. In our operational conditions (reactor geometry and flow rate), a diffusion limitation uptake coefficient threshold of $\sim 1.5 \cdot 10^{-5}$ is estimated according to the Cooney-Kim-Davis method [50,52,53]. Thus, uptake coefficients higher that $1.5 \cdot 10^{-5}$ are underestimated and should be considered as a lower limit. Despite this limitation, conclusions made on the observed tendency in this study remain valid. Uptake coefficients calculated for photocatalytic and reference paints with 53, 72 and 80 % PVC are summarized in Table 1.

Table 1: NO_2 uptake coefficients calculated according to equation (3). Experimental conditions were set to initial NO_2 mixing ratio of 40 ppb, RH 40 %, irradiation of 8.8 W m^{-2} (integrated between 340 and 400 nm), surface temperature of 23 °C.

	NO_2 Uptake coefficients	
PVC (%)	Reference paint	Photocatalytic paint
53	$(5.3\pm5)\cdot10^{-7}$	$(3.3\pm0.5)\cdot10^{-6}$
72[a]	$(1.6\pm0.2)\cdot10^{-6}$	$(1.7\pm0.1)\cdot10^{-5}$
80	$(4.7\pm0.5)\cdot10^{-6}$	$(2.7\pm0.1)\cdot10^{-5}$

[a]from Gandolfo et al (2015) [18]

The uptake coefficients of NO_2 on photocatalytic paint are 6, 11 and 6 times higher than the NO_2 uptake coefficients on reference paint for PVC of 53, 72 and 80 %, respectively.

3.2.1. Influence of the pigment volume concentration

Figure 3 shows the variation of NO_2 uptakes as a function of PVC for the reference paint and photocatalytic paint.

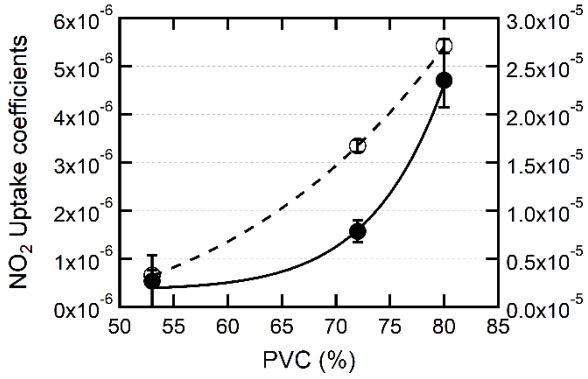

Figure 3: NO_2 uptake coefficients plotted against PVC. Uptakes were calculated in experiments under experimental conditions set as RH 40 %, irradiation 8.8 W m^{-2}, surface temperature 23 °C. Filled circles ((●) reference paint) refer to the left axis and empty circles ((○) photocatalytic paint) to the right axis. Lines correspond to best fits determined with Igor pro Wavemetrics software according to equation (4). Error bars are 1σ.

For both types of paints (reference and photocatalytic), PVC of 80 % shows the highest NO_2 uptake coefficient while PVC of 53 % shows the lowest reactivity. Results indicate that the NO_2 heterogeneous reactivity varies according to the PVC and thus to the porosity. On reference paints, the NO_2 uptake coefficients increases 3 times from $5.3 \cdot 10^{-7}$ (53 % PVC) to $1.6 \cdot 10^{-6}$ (72 % PVC). The NO_2 uptake coefficient for 80 % PVC increases one order of magnitude compared to the NO_2 uptake for 53 % PVC. Moreover, the uptake coefficient increases about one order of magnitude from $3.3 \cdot 10^{-6}$ for 53 % PVC to $2.7 \cdot 10^{-5}$ for 80 % PVC demonstrating that the porosity of the photocatalytic paint is an important factor for the NO_2 removal from ambient indoor air. The tendency observed in PVC dependence follows a power fit described by equation (4):

$$\gamma = \gamma_0 + A \times PVC^b \qquad (4)$$

where A is a pre-power factor. The coefficient from eq (4) is presented in Table 2.

Table 2: Factors experimentally determined according to equation (4)

	Reference paint	**Photocatalytic paint**
γ_0	$3.8 \cdot 10^{-7}$	$-2.0 \cdot 10^{-6}$
A	$1.5 \cdot 10^{-29}$	$3.6 \cdot 10^{-13}$
b	11.9	4.2

3.2.2. Influence of the relative humidity

Figure 4 shows the dependence of NO_2 uptake coefficients with RH for three different paint porosities, 53 % PVC, 72 % PVC, and 80 % PVC. It can be seen that for the porosity 53 % PVC, the NO_2 uptake coefficients increase with RH and reach their maximum at 30 to 40 % RH. Then, the uptake coefficients decrease with RH up to 70 %. A similar trend of dependence with RH was observed in our previous study on photocatalytic paint containing 7 % of nanoTiO_2 and a 72 % PVC under 20 W m^{-2} irradiation [18]. For comparison purpose these data from Gandolfo et al. are included in Figure 4.

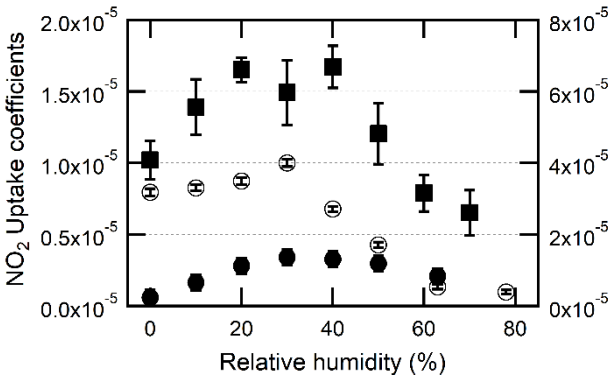

Figure 4: NO_2 uptake coefficients as a function of relative humidity (0-80 %) on photocatalytic paint containing 7 % of nanoTiO_2 under 8.8 w m^{-2} irradiation and a surface temperature of 23 °C. Filled circles and squares refer to the left axis and empty circles to the right axis. (●) 53 % PVC, (■) 72 % PVC, (○) 80 % PVC. Note that for the paint with PVC of 72 % (filled square), the light intensity was 20 W m^{-2}. Error bars are 1σ.

It is noticeable that on paint with PVC of 80 %, the influence of water in the lower range of RH is less important than for the other porosities of the paint. The uptake coefficients of NO_2 show a maximum value of about $4 \cdot 10^{-5}$ in the range of RH 0-30% and then rapidly decreases and reaches its minimum value of $1 \cdot 10^{-5}$ at RH 60 %.

3.3. By-products formation

The heterogeneous reaction of NO_2 on photocatalytic paints is an important source of HONO [18,43]. The two most important parameters influencing the HONO formation through this process are (1) the quantity of TiO_2 nanoparticles embedded in the paint and (2) the surface temperature of the painted walls. In this study, the yield of HONO formed upon heterogeneous conversion of NO_2 on photocatalytic paint (7 % TiO_2) at three different porosities, was observed at constant surface temperature of 23 °C and different RH. The obtained HONO formation yields are summarized in Table 3.

Table 3: HONO yields derived from the heterogeneous reaction of NO_2 (40 ppb) with photocatalytic paint containing 7% of TiO_2 nanoparticles under 8.8 w m^{-2} irradiation as a function of PVC.

	HONO yields (%)		
RH (%)	53 % PVC	72 % PVC [a]	PVC 80 %
0	9±5	*	*
10	46±18	4±1	4±2
20	41±6	13±3	4±1
30	29±9	15±4	7±1
40	31±18	12±6	2±1
50	7±1	*	3±1
60	*	*	*
80	*	*	*

[a]Under 20 W m^{-2} irradiation (Gandolfo et al (2015) [18])

*no production

In absence of RH, HONO is formed with a yield of 9 % only by the paint with 53 % PVC. On this paint, a maximum HONO yield is observed at low RH i.e. 46 % and 41 % at 10 and 20 % RH. Increasing the porosity of the paint leads to considerably lower HONO yields. The maximum HONO yield of 15 % and 7 %, was observed at 30 % RH on the paints with 72% PVC and 80 % PVC, respectively. It is worth noticing that at relatively higher RH (60 % and 80%) there is no HONO formation on the photocatalytic paints with all three different porosities (53 %, 72 % and 80 % PVC). Moreover, there is also no HONO formation on the reference paint. In fact, the reference paints acted as a sink of HONO. However, the HONO degradation on the paint is beyond the scope of this study and has not been further investigated. NO is another by-product formed in the NO_2 heterogeneous reactivity on photocatalytic paints (Table 4) [17,18].

Table 4: NO yields derived from the heterogeneous reaction of NO_2 (40 ppb) with the photocatalytic paint containing 7% of TiO_2 nanoparticles under 8.8 w m^{-2} irradiation as a function of PVC and RH.

	NO yields (%)		
RH (%)	53 % PVC	72 % PVC [a]	80 % PVC
0	*	*	*
10	*	7±7	10±2
20	*	31±4	44±4
30	12±3	33±4	55±15
40	3±4	29±7	65±11
50	*	*	50±21
60	*	*	*
80	*	*	*

[a]Under 20 W m^{-2} irradiation (Gandolfo et al (2015) [18]

*no production

On the photocatalytic paint with 53 % PVC, NO was formed with rather low yields of only 12 % and 3 % at 30 % and 40 % RH, respectively. However, relatively higher NO yields were observed on the paints with 72 % PVC and 80 % PVC in contrast with the low HONO yields observed on these paints. A maximum NO yield of 33 % and 65 % was observed on the paint with 72 % PVC at 30 % RH and on 80% PVC at 40 % RH, respectively. As for the HONO observations at higher RH (60 % and 80 %), NO is not formed on the photocatalytic paints with all three different porosities (53 %, 72 % and 80 % PVC). These observations indicate that the sum of the yield of both gas-phase products (NO + HONO) as a function of PVC increased from 46 % to 67 % suggesting a reduction of the condensed phase products such as nitrite and nitrate on the photocatalytic paints [17,54].

4. Discussion

4.1. Comparison of NO_2 uptake coefficients on various paint

In this study the NO_2 uptake coefficients on reference paints range from $5.3 \cdot 10^{-7}$ to $4.7 \cdot 10^{-6}$ which are higher than previously reported uptakes on commercially available paints exhibiting γ_{NO2} values from 1 to $4.7 \cdot 10^{-7}$. [55]. Different uptake coefficients in both studies may be explained by different binder composition, paints applications methods and experimental conditions. According to Langmuir-Hinshelwood mechanism [56], higher initial NO_2 mixing ratio implies lower uptake coefficients which could partially explain the uptake coefficient of 1 to $4 \cdot 10^{-7}$ for initial NO_2 of 60 ppb [55] compared to the observed γ_{NO2} in this study at initial NO_2 mixing ratio of 40 ppb.

The NO_2 degradation on photocatalytic paints is considerably higher in comparison with the reference paints in agreement with the literature data [15]. Depending on relative humidity (0-80 %) and under 8.8 W m^{-2} irradiation, NO_2 uptakes on photocatalytic paints range from 0.7 to $1.6 \cdot 10^{-6}$ and from 0.4 to $4 \cdot 10^{-5}$ for the photocatalytic paints with 53 and 80 % PVC, respectively. For the paint with 72 % PVC, the uptake coefficient under same irradiation conditions is $1.7 \cdot 10^{-5}$ at RH 40 %. Except for the paint with 53 % PVC, the uptake coefficients from this study are also in good agreement with Laufs et al

(2010) who observed uptakes between 0.5 and $3 \cdot 10^{-5}$ on commercial photocatalytic paints with unknown PVC and low nanoTiO_2 contents [17]. Furthermore, experiments on pure TiO_2 or TiO_2/SiO_2 surfaces show NO_2 uptakes of the order of 10^{-6} or smaller [57,58] in good agreement with those obtained on paint with 53 % PVC but much smaller than the γ_{NO2} measured on the paints with of 72% and 80 % PVC. These observations indicate that the paint porosity plays an important role for NO_2 removal by photocatalytic paints in agreement with previous observations on highly porous photocatalytic materials (paints, mortar or coatings) [20,24,33,34]. A more open surface texture allows increasing the specific surface area and surface adsorption capacities [31] which finally induce a better photocatalytic activity.

4.2. Proposed mechanism

Water plays a dual role in photocatalytic activity. On one hand, its presence promotes the formation of very reactive adsorbed OH radicals on semi-conductors through reactions (5) and (6):

$$TiO_2 \xrightarrow{h\upsilon} h_{vb}^{+} + e_{cb}^{-} \quad (5)$$

$$h_{vb}^{+} + H_2O \rightarrow OH + H^{+} \quad (6)$$

On the other hand, water co-adsorption on active site compete with NO_2 adsorption. In this study an optimum NO_2 photocatalytic remediation was observed in the range of 30 % to 50 % RH, depending on the porosity (Figure 4). Under dry conditions, NO_2 uptakes are much lower, confirming the role of water molecules in the NO_2 removal process. This process was especially pronounced for the paints with 53 % and 72 % PVC rather than for the paint with 80 % PVC where almost no effect was observed. At RH higher than 50 %, NO_2 uptakes decrease most probably because of the shielding effect and co-adsorption of water molecules. This observation is in agreement with the RH dependent photocatalytic NO_2 degradation on various surfaces: paints [17,19] or pure TiO_2 [59]. However, El Zein an Bedjanian (2012) did not observe any effect of water molecules on NO_2 reactivity on pure TiO_2 surface. [58]. Interestingly, we observed that the maximum NO_2 uptake is shifted to higher RH as the PVC decreased (maximum uptakes are observed at RH 50 %, 40 % and 30 % for paints with of 53, 72 and 80 % PVC respectively). In other words, the competition between NO_2 and water molecules for

the adsorption on the surface becomes stronger as the paint becomes more porous. The reason for this remains unclear, however, a suggestion to explain this phenomenon is proposed below. The increase of the porosity is achieved through lowered organic binder quantity. Thus, calcium carbonate components are more exposed to the moisture as the PVC is higher (Figure 1). The organic matter is less hydrophilic than calcium carbonate, implying that decrease of PVC means increase of the organic coating, which in turn should drive the paint to a more hydrophobic surface. Moreover, the water layers are better formed on hydrophilic surface than hydrophobic surfaces. Thus, the establishment of water layer(s) on the surface is shifted for higher RH and could thus explain our observations. In addition, at 25 °C, gaseous H_2O and NO_2 diffusion coefficients are 0.28 and 0.16 $cm^2\ s^{-1}$, respectively [60,61]. If we assume that H_2O and NO_2 diffusion ratio remains stable in the pores, the higher diffusion coefficient of water molecule could facilitate its penetration in microstructure as pores in comparison with NO_2 molecules and thus be competitive for lower RH.

Interestingly, HONO and NO yields are dependent on PVC. At low porosity, HONO formation is promoted while increased porosity led to the formation of NO instead of HONO. We previously proposed the formation of HONO and NO on photocatalytic paints through the set of reactions (5) to (10) [18].

$$e_{cb}^- + O_2 \rightarrow O_2^- \quad (7)$$

$$NO_2 + O_2^-(+H^+) \rightarrow NO_2^-(HONO) + O_2 \quad (8)$$

$$NO_2(ads) \xrightarrow{+h\nu, TiO_2} NO(ads) + O(^3P) \quad (9)$$

$$NO(ads) + OH(ads) \xrightarrow{TiO_2} HONO \quad (10)$$

In this study, on photocatalytic paint with PVC of 53 %, HONO yield was almost 50 % at RH of 10-20 %. On this paint, increase of RH up to 50 % favored NO_2 uptakes but inhibited HONO formation indicating a non-photocatalytic process involved in the HOHO formation on this paint. This high $NO_2 \rightarrow$HONO conversion ratio, is in good agreement with HONO

yield estimated by Bartolomei et al. (2014) on standard commercial paint [40]. The authors [41] suggested a photo-induced NO_2 reaction on organic materials partially responsible for HONO formation as proposed by Stemmler et al (2006) [62] and further confirmed by Liu et al (2019) [63] which could be also the case in this study. The observed high HONO yield of 50 % is in contrast with the observed HONO yields on building photocatalytic materials as concretes or paints where very weak or no HONO production was observed [17,18,54]. Regarding the NO as a by-product the higher porosity induces higher NO production. As observed in Figure 4, the role of water molecules in the lower range of RH (0 to 40 %) on NO_2 photocatalytic elimination is reduced for the paint at PVC of 80 %. We observed an almost constant reactivity, indicating a diminution of the role of reaction (6) and consequently (8). Presumably, NO_2 degradation occurred via reaction (9) producing NO. NO(ads) recombined with OH to form HONO to a lesser extent (10). Nevertheless, the proposed mechanism above cannot explain all the observation. Intuitively, the increased porosity should increase the contact time between the pollutants and the photocatalyst thus promoting oxidation products such as nitric acid (HNO_3). This suggestion is contradicted by the increased NO-HONO yield which increases from lower to higher PVC. Further studies are needed to better understand the formation process of NO and HONO on porous photocatalytic paints.

4.3. Environmental implications

As mentioned above, the NO_2 is more efficiently removed from the gas phase in contact with porous photocatalytic paints giving a certain advantage for indoor applications. In addition, the formation of HONO which is considered as a harmful compound and a major player in the oxidative capacity of indoor air is reduced as the paint porosity increase [64–69]. NO is relatively inert in comparison to NO_2 or HONO and its presence is preferable instead of both other nitrogen compounds. However, in organic photocatalytic paints, the binder is consumed

by redox reactions occurring on semiconductor surface releasing high amounts of highly volatile and oxidized short carbonaceous compounds [15,26]. Recently, in our group, VOCs surface emission fluxes (SEF) of various VOCs have been estimated by proton transfer reaction mass spectrometer (PTR-MS) connected at the outlet of the flow tube reactor [26,70]. As mentioned above (section 3.1), porosity variation is induced by changes in binder volume. Thus, it is expected that porosity variation influence VOCs surface emission fluxes because the photocatalytic degradation of the binder leads to the VOCs release in the ambient air. The SEF of formaldehyde and acetaldehyde are presented in Figure 5 as a function of PVC at 40 % of RH and under 8.8 W m^{-2} irradiation.

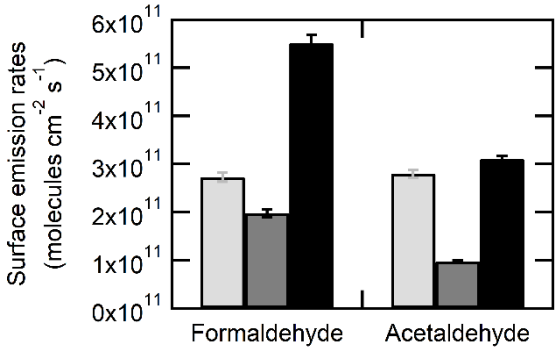

Figure 5: Surface emission fluxes of formaldehyde and acetaldehyde released by the photocatalytic paint (7 % of TiO_2 nanoparticles) at 40 % RH, under 8.8 W m^{-2} irradiation and 23°C surface temperature. Light gray, gray and black bars correspond to emissions of paint with PVC 53, 72 and 80 % respectively.

It can be seen that both SEF are PVC dependent. The minimum is observed for the paint with 72 % PVC with SEF of $(2.0 \pm 0.1)\cdot10^{11}$ and $(9.8 \pm 0.3)\cdot10^{10}$ molecules cm^{-2} s^{-1} for formaldehyde and acetaldehyde respectively. The maximum formaldehyde SEF was $(5.5 \pm 0.2)\cdot10^{11}$ molecules cm^{-2} s^{-1} at 80 % PVC while at 53 % PVC, surface emission flux was $(2.7 \pm 0.1)\cdot10^{11}$ molecules cm^{-2} s^{-1}. Regarding acetaldehyde emission, the maximum is shared at 53 and 80 % PVC with surface emission fluxes closed to $3\cdot10^{11}$ molecules cm^{-2} s^{-1}.

Increasing the PVC from 53 % to 72 %, lowered VOCs emission by reducing the quantity of organic material potentially alterable. Further, the increase of PVC would lead to an increase of SEF of formaldehyde and acetaldehyde. Opening and lightening the texture may facilitate desorption of VOCs and/or weaken the structure of the paint. Recently, simple model estimations have shown that the mixing ratios of formaldehyde and acetaldehyde in a typical indoor environment are 18 and 14 times higher, respectively, in presence of photocatalytic paints (7 %nanoTiO_2) in comparison to the reference paint [26]. Implementing SEF for formaldehyde and acetaldehyde from photocatalytic paints with 80 % PVC results in 41 and 47 times higher mixing ratios, respectively, than from reference paints. The calculated mixing ratios (41 and 42 ppb for formaldehyde and acetaldehyde respectively) exceed the threshold value of 34 μg m^{-3} (28 ppb in the U.S. Standard Conditions for Temperature and Pressure) in California and the threshold value of 10 μg m^{-3} (8 ppb in the U.S. Standard Conditions for Temperature and Pressure) in France. While the removal of NO_2 is quantitatively improved from a factor of 2 to 3 by increasing porosity, the amount of formaldehyde and acetaldehyde released act as a major obstacle in a safe-by-design photocatalytic paint production. However, recent advances in binder modification (use of mineral binders instead of organics) shown an important decrease of VOCs emission [70]. The combination of both parameters, the porosity and the mineral binder, toward NOx abatement and VOC released could considerably help the performance of photocatalytic paint for indoor air remediation. However, to date, we can only support the needs of careful investigations on photocatalytic paints on NOx abatement but also on by-products formations as proposed by Ifang et al. (2014) [51] and performed here.

References

[1] C.J. Weschler, N. Carslaw, Indoor Chemistry, Environ. Sci. Technol. 52 (2018) 2419–2428.

[2] The WHO European Centre for Environment and Health, WHO Guidelines for indoor air quality: selected pollutants, 9 (2010) 454.

[3] United States Environmental Protection Agency, Introduction to Indoor Air Quality, (n.d.). https://www.epa.gov/indoor-air-quality-iaq/introduction-indoor-air-quality

[4] ANSES-the French Agency for Food Environmental and Occupational Health & Safety, Study of the socio-economic cost of indoor air pollutants, 2014.

[5] D. Crump, A. Dengel, M. Swainson, Indoor air quality in highly energy efficient homes-a review Housing research in partnership with BRE Trust, 2009. www.nhbcfoundation.org

[6] J. Sundell, H. Levin, W.W. Nazaroff, W.S. Cain, W.J. Fisk, D.T. Grimsrud, F. Gyntelberg, Y. Li, A.K. Persily, A.C. Pickering, J.M. Samet, J.D. Spengler, S.T. Taylor, C.J. Weschler, Ventilation rates and health: multidisciplinary review of the scientific literature, Indoor Air. 21 (2011) 191–204.

[7] A.L. Linsebigler, G. Lu, J.T. Yates, Photocatalysis on TiO_2 Surfaces: Principles, Mechanisms, and Selected Results, Chem. Rev. 95 (1995) 735–758.

[8] K. Nakata, A. Fujishima, TiO_2 photocatalysis: Design and applications, J. Photochem. Photobiol. C Photochem. Rev. 13 (2012) 169–189.

[9] J. Ângelo, L. Andrade, L.M. Madeira, A. Mendes, An overview of photocatalysis phenomena applied to NOx abatement, J. Environ. Manage. 129 (2013) 522–539.

[10] J. Schneider, M. Matsuoka, M. Takeuchi, J. Zhang, Y. Horiuchi, M. Anpo, D.W. Bahnemann, Understanding TiO_2 Photocatalysis: Mechanisms and Materials, Chem. Rev. 114 (2014) 9919–9986.

[11] C. George, A. Beeldens, F. Barmpas, J.F. Doussin, G. Manganelli, H. Herrmann, J. Kleffmann, A. Mellouki, Impact of photocatalytic remediation of pollutants on urban air quality, Front. Environ. Sci. Eng. 10 (2016).

[12] C. Byrne, G. Subramanian, S.C. Pillai, Recent advances in photocatalysis for environmental applications, J. Environ. Chem. Eng. 6 (2018) 3531–3555.

[13] Z. Shayegan, C.-S. Lee, F. Haghighat, TiO_2 photocatalyst for removal of volatile organic compounds in gas phase – A review, Chem. Eng. J. 334 (2018) 2408–2439.

[14] M.R. Hoffmann, S.T. Martin, W. Choi, D.W. Bahnemann, Environmental applications of semiconductor photocatalysis, Chem. Rev. 95 (1995) 69–96.

[15] T. Salthammer, F. Fuhrmann, Photocatalytic surface reactions on indoor wall paint, Environ. Sci. Technol. 41 (2007) 6573–6578.

[16] J. Auvinen, L. Wirtanen, The influence of photocatalytic interior paints on indoor air quality, Atmos. Environ. 42 (2008) 4101–4112.

[17] S. Laufs, G. Burgeth, W. Duttlinger, R. Kurtenbach, M. Maban, C. Thomas, P. Wiesen, J. Kleffmann, Conversion of nitrogen oxides on commercial photocatalytic dispersion paints, Atmos. Environ. 44 (2010) 2341–2349.

[18] A. Gandolfo, V. Bartolomei, E. Gomez Alvarez, S. Tlili, S. Gligorovski, J. Kleffmann, H. Wortham, The effectiveness of indoor photocatalytic paints on NOx and HONO levels, Appl. Catal. B Environ. 166–167 (2015).

[19] T. Maggos, J.G. Bartzis, P. Leva, D. Kotzias, Application of photocatalytic technology for NOx removal, Appl. Phys. A. Gen. 89 (2007) 81–84.

[20] N.S. Allen, M. Edge, J. Verran, L. Caballero, C. Abrusci, J. Stratton, J. Maltby, C. Bygott, Photocatalytic Surfaces: Environmental Benefits of Nanotitania, Open Mater. Sci. J. 3 (2009) 6-27.

[21] J. Ângelo, L. Andrade, A. Mendes, Highly active photocatalytic paint for NOx abatement under real-outdoor conditions, Appl. Catal. A, Gen. 484 (2014) 17–25.

[22] B. Tryba, P. Homa, R.J. Wróbel, A.W. Morawski, Photocatalytic decomposition of benzo-[a]-pyrene on the surface of acrylic, latex and mineral paints. Influence of paint composition, J. Photochem. Photobiol. A Chem. 286 (2014) 10–15.

[23] Q.L. Yu, Y. Hendrix, S. Lorencik, H.J.H. Brouwers, Field study of NOx degradation by a mineral-based air purifying paint, Build. Environ. 142 (2018) 70–82.

[24] C. Águia, J. Ângelo, L.M. Madeira, A. Mendes, Photo-oxidation of NO using an exterior paint - Screening of various commercial titania in powder pressed and paint films, J. Environ. Manage. 92 (2011) 1724–1732.

[25] O. Geiss, C. Cacho, J. Barrero-Moreno, D. Kotzias, Photocatalytic degradation of organic paint constituents-formation of carbonyls, Build. Environ. 48 (2012) 107–112.

[26] A. Gandolfo, S. Marque, B. Temime-Roussel, R. Gemayel, H. Wortham, D. Truffier-Boutry, V. Bartolomei, S. Gligorovski, Unexpectedly High Levels of Organic Compounds Released by Indoor Photocatalytic Paints, Environ. Sci. Technol. 52 (2018) 11328–11337.

[27] H. Dong, G. Zeng, L. Tang, C. Fan, C. Zhang, X. He, Y. He, An overview on limitations of TiO_2 -based particles for photocatalytic degradation of organic pollutants and the corresponding countermeasures, Water Res. 79 (2015) 128–146.

[28] C.H. Ao, S.C. Lee, Indoor air purification by photocatalyst TiO_2 immobilized on an activated carbon filter installed in an air cleaner, Chem. Eng. Sci. 60 (2005) 103–109.

[29] S. Morales-Torres, L.M. Pastrana-Martínez, J.L. Figueiredo, J.L. Faria, A.M.T. Silva, Design of graphene-based TiO 2 photocatalysts-a review, Env. Sci Pollut Res. 19 (2012) 3676–3687.

[30] I. Jansson, S. Suárez, F.J. Garcia-Garcia, B. Sánchez, Zeolite-TiO_2 hybrid composites for pollutant degradation in gas phase, Appl. Catal. B Environ. 178 (2015) 100–107.

[31] C. Giosuè, A. Belli, A. Mobili, B. Citterio, F. Biavasco, M. Ruello, F. Tittarelli, Improving the Impact of Commercial Paint on Indoor Air Quality by Using Highly Porous Fillers, Buildings. 7 (2017) 110.

[32] R. Sugrañez, J.I. Álvarez, M. Cruz-Yusta, I. Mármol, J. Morales, L. Sánchez, Controlling microstructure in cement based mortars by adjusting the particle size distribution of the raw materials, Constr. Build. Mater. 41 (2013) 139–145.

[33] R. Sugrañez, J.I. Álvarez, M. Cruz-Yusta, I. Mármol, J. Morales, J. Vila, L. Sánchez, Enhanced photocatalytic degradation of NO x gases by regulating the microstructure of mortar cement modified with titanium dioxide, Build. Environ. 69 (2013) 55–63.

[34] R. Zouzelka, J. Rathousky, Photocatalytic abatement of NOx pollutants in the air using commercial functional coating with porous morphology, Appl. Catal. B Environ. 217 (2017) 466–476.

[35] M.E. Monge, B. D'Anna, L. Mazri, A. Giroir-Fendler, M. Ammann, D.J. Donaldson, C. George, Light changes the atmospheric reactivity of soot, Proc. Natl. Acad. Sci. 107 (2010) 6605–6609.

[36] R. Ammar, M.E. Monge, C. George, B. D'Anna, Photoenhanced NO_2 loss on simulated urban grime, Phys. Chem. Chem. Phys. 11 (2010) 3956–3961.

[37] T. Bartels-Rausch, M. Brigante, Y.F. Elshorbany, M. Ammann, B. D'Anna, C. George, K. Stemmler, M. Ndour, J. Kleffmann, Humic acid in ice: Photo-enhanced conversion of nitrogen dioxide into nitrous acid, Atmos. Environ. 44 (2010) 5443–5450.

[38] M.E. Monge, B. D'Anna, C. George, Nitrogen dioxide removal and nitrous acid formation on titanium oxide surfaces—an air quality remediation process?, Phys. Chem. Chem. Phys. 12 (2010) 8991–8998.

[39] C. George, R.S. Strekowski, J. Kleffmann, K. Stemmler, M. Ammann, Photoenhanced uptake of gaseous NO_2 on solid organic compounds: a photochemical source of HONO?, Faraday Discuss. 130 (2005) 195.

[40] V. Bartolomei, M. Sörgel, S. Gligorovski, E.G. Alvarez, A. Gandolfo, R. Strekowski, E. Quivet, A. Held, C. Zetzsch, H. Wortham, Formation of indoor nitrous acid (HONO) by light-induced NO_2 heterogeneous reactions with white wall paint, Environ. Sci. Pollut. Res. 21 (2014) 9259–9269.

[41] E. Gómez Alvarez, M. Sörgel, S. Gligorovski, S. Bassil, V. Bartolomei, B. Coulomb, C. Zetzsch, H. Wortham, Light-induced nitrous acid (HONO) production from NO_2 heterogeneous reactions on household chemicals, Atmos. Environ. 95 (2014) 391–399.

[42] A. Gandolfo, L. Rouyer, H. Wortham, S. Gligorovski, The influence of wall temperature on NO_2 removal and HONO levels released by indoor photocatalytic paints, Appl. Catal. B Environ. 209 (2017) 429–436.

[43] A. Gandolfo, L. Rouyer, H. Wortham, S. Gligorovski, The influence of wall temperature on NO2removal and HONO levels released by indoor photocatalytic paints, Appl. Catal. B Environ. 209 (2017) 429–436.

[44] Labex SERENADE: Safe(r) ecodesign research and education applied to nanomaterial development. http://www.labex-serenade.fr/

[45] D. Truffier-Boutry, B. Fiorentino, V. Bartolomei, R. Soulas, O. Sicardy, A. Benayad, J.F. Damlencourt, B. Pépin-Donat, C. Lombard, A. Gandolfo, H. Wortham, G. Brochard, A. Audemard, L. Porcar, G. Gebel, S. Gligorovski, Characterization of photocatalytic paints: A relationship between the photocatalytic properties-release of nanoparticles and volatile organic compounds, Environ. Sci. Nano. 4 (2017) 1998–2009.

[46] ISO 4618-1 Paints and varnishes - Terms and definiations for coating materials - Part 1: General terms, 1998. https://www.sis.se/api/document/preview/611796/

[47] J. Heland, J. Kleffmann, R. Kurtenbach, P. Wiesen, A new instrument to measure gaseous nitrous acid (HONO) in the atmosphere, Environ. Sci. Technol. 35 (2001) 3207–3212.

[48] J. Kleffmann, J.C. Lörzer, P. Wiesen, C. Kern, S. Trick, R. Volkamer, M. Rodenas, K. Wirtz, Intercomparison of the DOAS and LOPAP techniques for the detection of nitrous acid (HONO), Atmos. Environ. 40 (2006) 3640–3652.

[49] J. Kleffmann, J. Heland, R. Kurtenbach, J. Lorzer, P. Wiesen, A new instrument (LOPAP) for the detection of nitrous acid (HONO), Environ. Sci. Pollut. Res. 9(4) (2002) 48–54.

[50] D.M. Murphy, D.W. Fahey, Mathematical treatment of the wall loss of a trace species in denuder and catalytic converter tubes, Anal. Chem. 59 (1987) 2753–2759.

[51] S. Ifang, M. Gallus, S. Liedtke, R. Kurtenbach, P. Wiesen, J. Kleffmann, Standardization methods for testing photo-catalytic air remediation materials: Problems and solution, Atmos. Environ. 91 (2014) 154–161.

[52] D. 0. Cooney, S.-S. Kim, E.J. Davis, Analyses of mass transfer in hemodialyzers for laminar blood flow and homogeneous dialysate, Chem. Eng. Sci. 29 (1974) 1731–1738.

[53] W. Behnke, C. George, V. Scheer, C. Zetzsch, Production and decay of ClNO2 from the reaction of gaseous N2O5 with NaCl solution: Bulk and aerosol experiments, J. Geophys. Res. Atmos. 102 (1997) 3795–3804.

[54] F. Mothes, S. Ifang, M. Gallus, B. Golly, A. Boréave, R. Kurtenbach, J. Kleffmann, C. George, H. Herrmann, Bed flow photoreactor experiments to assess the photocatalytic nitrogen oxides abatement under simulated atmospheric conditions, Appl. Catal. B Environ. 231 (2018) 161–172.

[55] V. Bartolomei, M. Sörgel, S. Gligorovski, E.G. Alvarez, A. Gandolfo, R. Strekowski, E. Quivet, A. Held, C. Zetzsch, H. Wortham, Formation of indoor nitrous acid (HONO) by light-induced NO_2 heterogeneous reactions with white wall paint, Environ. Sci. Pollut. Res. 21 (2014) 9259–9269.

[56] B.J. Finlayson-Pitts, J.N. Pitts, Chemistry of the Upper and Lower atmosphere. Theory, Experiments, and Application, Acad. Press. San Diego. (2000).

[57] M. Ndour, B. D'Anna, C. George, O. Ka, Y. Balkanski, J. Kleffmann, K. Stemmler, M. Ammann, Photoenhanced uptake of NO_2 on mineral dust: Laboratory experiments and model simulations, Geophys. Res. Lett. 35 (2008).

[58] A. El Zein, Y. Bedjanian, Interaction of NO_2 with TiO_2 surface under UV irradiation: measurements of the uptake coefficient, Atmos. Chem. Phys. 12 (2012) 1013–1020.

[59] C.H. Ao, S.C. Lee, C.L. Mak, L.Y. Chan, Photodegradation of volatile organic compounds (VOCs) and NO for indoor air purification using TiO_2: promotion versus inhibition effect of NO, Appl. Catal. B Environ. 42 (2003) 119–129.

[60] E.L. Cussler, Diffusion : mass transfer in fluid systems, Cambridge University Press, 2009.

[61] J.N. Cape, Review of the use of passive diffusion tubes for measuring concentrations of nitrogen dioxide in air, 2005.

[62] K. Stemmler, M. Ammann, C. Donders, J. Kleffmann, C. George, Photosensitized reduction of nitrogen dioxide on humic acid as a source of nitrous acid, Nature. 440 (2006) 195–198.

[63] J. Liu, S. Li, M. Mekic, H. Jiang, W. Zhou, G. Loisel, Photoenhanced Uptake of NO_2 and HONO Formation on Real Urban Grime, Environ. Sci. Technol. Lett. 6 (2019) 413–417.

[64] M. Sleiman, L.A. Gundel, J.F. Pankow, P. Jacob, B.C. Singer, H. Destaillats, Formation of carcinogens indoors by surface-mediated reactions of nicotine with nitrous acid, leading to potential thirdhand smoke hazards, Proc. Natl. Acad. Sci. 107 (2010) 6576–6581.

[65] E. Gómez Alvarez, D. Amedro, A. Charbel, S. Gligorovski, C. Schoemaecker, C. Fittschen, J.-F. Doussin, H. Wortham, Unexpectedly high indoor hydroxyl radical concentrations associated with nitrous acid, Proc. Natl. Acad. Sci. 110 (2013) 13294–13299.

[66] J.N.J. Pitts, Photochemical and biological implication of atmospheric reaction of amines and benzo(a)pyrene, Philos. Trans. R. Soc. A. 290 (1979) 551–576.

[67] J.J. Kirchner, P.B. Hopkins, Nitrous acid cross-links duplex DNA fragments through deoxyguanosine residues at the sequence 5’-CG, J. Am. Chem. Soc. 113 (1991) 4681–4682.

[68] S. Gligorovski, Nitrous acid (HONO): An emerging indoor pollutant, J. Photochem. Photobiol. A Chem. 314 (2016) 1–5.

[69] S. Gligorovski, J.P.D. Abbatt, An indoor chemical cocktail, Science. 359 (2018) 632–633.

[70] J. Morin, A. Gandolfo, B. Temime-Roussel, R. Strekowski, G. Brochard, V. Bergé, S. Gligorovski, H. Wortham, Application of a mineral binder to reduce VOC emissions from indoor photocatalytic paints, Build. Environ. 156 (2019) 225–232.